Double Fed Induction Generator Shaft Misalignment Monitoring by FBG Frame Strain Sensing

Yingzhao Wang, Anees Mohammed, Nur Sarma, and Siniša Djurović, *Member, IEEE*

***Abstract*—This study explores the potential for using FBG strain sensing to enable recognition of the shaft misalignment condition in electric machine drivetrains through observation of machine frame distributed relative strain. The sensing principles, design and installation methods of the proposed technique are detailed in the paper. The scheme was applied on a purpose built wind turbine generator representative laboratory test rig and its performance evaluated in an extensive experimental study involving a range of healthy and misaligned shaft operating conditions. The obtained experimental data demonstrate the reported method's capability to enable recognition of generator shaft misalignment conditions and thus its health monitoring. Finally, it is shown that the thermal variation of the generator frame structure inherent to its operation, combined with the FBG sensor intrinsic thermo-mechanical cross sensitivity, has no detrimental impact on the fidelity and usability of the observed strain measurements.**

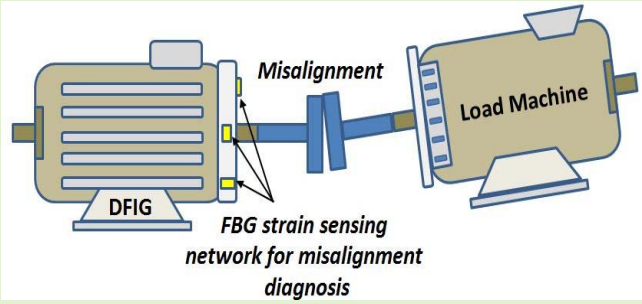

***Index Terms*— Electric machines, FBG sensors, misalignment monitoring, strain sensing, wind turbine generators.**

I. Introduction

OFFSHORE wind generation is increasingly seen as a dominant factor in decarbonizing our power supply and is set to become the largest source of electricity in the European Union by 2040 [1]. With wind turbines (WTs) growing in size and power capacity to exploit the higher and more consistent wind resource offshore, their exposure to harsh ambient conditions in remote offshore locations creates challenges for operation and maintenance (O&M): access is often limited and maintenance costly due to complicated repair infrastructure requirements imposed by the device location and scale. The development of WT in-service monitoring techniques that can assist maintenance decisions is thus of considerable importance as it can improve availability and reduce the high O&M cost [2] – this is currently estimated to account for up to 30% of total offshore farm lifetime cost, where the turbine drivetrain O&M expense is a major contributor [3]. The offshore wind O&M industry in the UK alone is anticipated to form an industry worth £2 billion/year nationally by 2025 [4], [5]: much of the needed cost savings in this area are believed to be possible through implementation of better proactive maintenance techniques underpinned by improved condition monitoring solutions [6]. In this regard, the relevant standards for wind turbine certification [7] require turbine drivetrains to be equipped with suitable monitoring systems to enable the understanding of its key components' integrity (e.g. bearings, generator, gearbox) with most manufacturers expanding these with proprietary systems aimed at enabling the monitoring of a wider array of drivetrain and associated device failure modes [6].

Shaft misalignment is estimated to contribute to up to 50% of all rotating machinery breakdowns [8] and can result in considerable downtime and economic losses if it is not detected timely. Misalignment is defined as a condition in which the shaft of the driving machine and that of the driven machine do not align with the same centerline. While ensuring accurate alignment can in principle prevent a considerable number of breakdowns, including the associated unplanned downtime and production loss, in practice the alignment is challenging to sustain over extended service periods and ideally needs continuous monitoring, as it is unavoidably compromised by a number of drivetrain inherent factors.

Manuscript received March 19, 2020; accepted March 22, 2020. Date of publication March 30, 2020; date of current version July 6, 2020. This work was supported by the U.K. Engineering and Physical Sciences Research Council HOME-Offshore: Holistic Operation and Maintenance for Energy From Offshore Wind Farms Consortium under Grant EP/P009743/1. The associate editor coordinating the review of this article and approving it for publication was Dr. Daniele Tosi. *(Corresponding author: Siniša Djurović.)*

Yingzhao Wang, Anees Mohammed, and Siniša Djurović are with the Electrical and Electronic Engineering Department, University of Manchester, Manchester M13 9PL, U.K. (e-mail: Sinisa.Durovic@manchester.ac.uk).

Nur Sarma is with the Department of Electrical and Electronic Engineering, Düzce University, Konuralp/Merkez, 81620 Duzce, Turkey.

Digital Object Identifier 10.1109/JSEN.2020.2984309

In WT systems in particular, shaft misalignment can give rise to undesirable forces leading to damage or destruction of bearings, seals, couplings, and eventually the gearbox and the generator [9]. Misalignment monitoring and diagnosis is thus especially important in contemporary WT drivetrains where due to additional issues associated with the remote and harsh operating environment misalignment issues have particularly significant downtime and repair cost implications [2], [10].

In modern WT field applications drivetrain online monitoring systems are legally required [11]; these typically use piezoelectric accelerometers for distributed monitoring of the drivetrain vibration and can achieve misalignment detection through observation of vibration components at shaft rotational speed multiples [8], [12]. In addition, generator alignment is typically inspected once every twelve months using costly laser alignment tools as part of a maintenance program periodic checks to ascertain existing misalignment levels and identify any required corrective action; these laser sensors are however not fully suitable for continuous monitoring [13]. While effective, the vibration based monitoring techniques can suffer in diagnostic reliability due to generator transient operation and limitations in dynamic range [10], hence alternative methods for shaft misalignment online monitoring are continuously researched: infra-red thermometers were applied in [10] to observe coupling temperature, but found to be sensitive to other heat sources in the drivetrain. Using generator current sensor measurements for misalignment detection was also explored [14], but was shown to be challenging as other fault modes can be confused with misalignment. Strain gauge application to measure displacement in vicinity of couplings was researched in [15], but found to be constrained by the sensor location requirements. Laser based shaft distance measurement was explored in [16], but requires further research to fully evaluate.

The application of fibre optic sensing for electric machine condition monitoring is increasingly developing as a promising alternative to conventional techniques [17]–[27]. The fibre Bragg grating (FBG) technology in particular presents a number of features which are attractive in this respect [28], [29]: Electromagnetic interference (EMI) immunity, small size and flexibility, multiplexing capability and that of multi-physical sensing. A number of FBG applications for electrical machine condition monitoring have recently been researched demonstrating promising potential. For example, FBG strain sensing use was explored for dynamic eccentricity, winding and broken bar detection in induction machines in [17]–[19], while FBG thermal sensing application for winding temperature monitoring and fault detection in permanent magnet and induction machines was studied in [20]–[22]. The development and application of FBG magnetic sensors for electric machine monitoring and diagnostic purposes was explored in [23]–[25], while [26] studies simultaneous use of single FBG head multiphysical sensing properties for machine bearing monitoring and [27] investigates the design of an FBG sensing suite for machine multi-parameter monitoring. The potential of FBG sensing application evaluation for misalignment monitoring in electric machine drivetrains however remains to be explored.

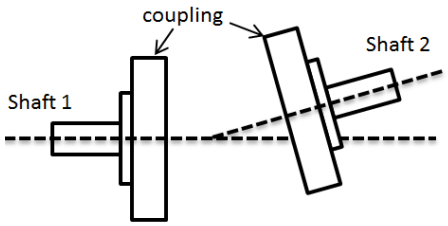

Fig. 1. Angular shaft misalignment - illustration.

In this study, FBG sensors are used to measure distributed relative strain on the generator frame surface to explore the potential of its monitoring to be used as a diagnostic tool for shaft misalignment detection. The paper first presents the utilized sensor design and installation procedure, and discusses the considered monitoring points of interest for this application. An experimental study is then undertaken on a purpose built double-fed induction generator (DFIG) test facility, which allows for controlled introduction of a number of levels of misalignment in tests. The DFIG topology is one of most commonly used in WT drivetrains [2] and was thus selected as representative of a typical WT drivetrain for the purpose of this study. The distributed FBG sensor suite was installed on the test generator frame and its performance evaluated in a range of tests involving various operating points in healthy and multiple different degrees of shaft misalignment operating conditions.

The attained results were then analysed, with particular attention to the location and orientation of individual FBG heads' influence on efficacy of capturing the diagnostic content in the measured strain signal; the findings were corroborated with a conventional vibration sensing technique using a commercial acceleration monitoring platform installed on the test generator. Further tests were then undertaken to ascertain the influence of thermal-cross sensitivity effects caused by the generator frame inherent change of thermal conditions on the analysed strain measurements. The presented findings demonstrate a strong potential of frame embedded FBG strain sensing application for enabling the recognition of shaft misalignment conditions in the wide operating range of the examined generator, and characterise the sensor orientation and placement sensitivity to fault induced excitation.

II. Shaft Misalignment

A. Mechanical Effects

In general, the shaft misalignment condition can be classified as: parallel (or offset) misalignment, angular misalignment or the combination of the two. This section revises the mechanical features of coupled rotating shaft behavior in presence of angular misalignment (illustrated in Fig.1), with a view to identifying mechanical disturbances that can originate from this condition.

Angular shaft misalignment can generally be represented by a simplified system that includes the universal joint model, illustrated in Fig. 2 [30]: here, the misalignment angle, β, and the motor position angle, θ_m, are used to define angular misalignment. In Fig. 2: θ_l is the load side shaft angular

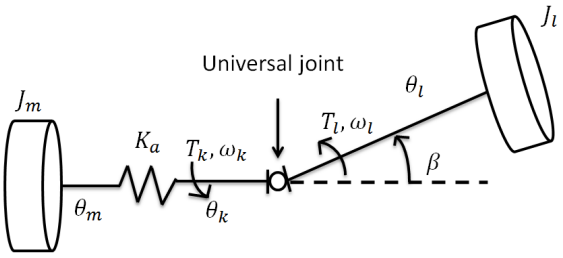

Fig. 2. Shaft misalignment universal joint based mode.

position, θ_k is the auxiliary angle defined to represent the joint transmitted rotational angular position on the motor side, ω_l and ω_k are the joint load side and motor side shaft angular speed, T_l and T_k are the joint load side and motor side shaft torque, J_m and J_l are the motor and load inertia, and K_a is the flexible coupling elasticity constant.

The simplified model enables analytical analysis of the general nature of the torque signal and thus the counterpart vibration signal disturbances arising from the presence of angular misalignment. The fundamental kinematic relations for the universal joint are well established and give the relationship between load and motor shafts angular displacements, θ_l and θ_k, for a β degrees misaligned joint [31]–[33]:

$$\theta_k = \tan^{-1}\left(\frac{1}{cos\beta} tan\theta_l\right) \tag{1}$$

The motor shaft angular speed is obtained by differentiation of the angle expression in (1) to yield:

$$\omega_k = \frac{cos\beta}{1-(sin\beta)^2\,(cos\theta_l)^2}\omega_l \tag{2}$$

Assuming the invariance of power between the load and the motor side allows the expression relating load and motor side torques and speeds to be written:

$$T_k\omega_k = T_l\omega_l \tag{3}$$

The torque transmitted from the load to the motor side via the misaligned universal joint model is obtained by substitution of equation (2) into equation (3) to give:

$$T_k = \frac{1-(sin\beta)^2\,(cos\theta_l)^2}{cos\beta} T_l, \tag{4}$$

which can conveniently be rearranged to the following term:

$$T_k = \left(\frac{1}{cos\beta} - \frac{\sin^2\beta}{2cos\beta} - \frac{\sin^2\beta}{2cos\beta} cos2\theta_l\right) T_l \tag{5}$$

Defining, for clarity, the load angular displacement $\theta_l = 2\pi f_r t$, where f_r is the load shaft fundamental rotational frequency ($f_r = \omega_r/2\pi$) it becomes apparent that the presence of angular misalignment will fundamentally give rise to torque signal pulsations at twice the rotational speed frequency (e.g. $2f_r$). Torque pulsations are usually expected to be transferred into counterpart machine frame vibration at identical frequencies [34] and can thus generally be expected to be possible to manifest as identical frequency frame deformation (strain) [19], [35], [36]. Furthermore, the general practice and research on angular misalignment monitoring indicated that increased frame vibration at fundamental rotational frequency is also possible with angular misalignment [37], [38].

B. Monitoring Practice

The common industrial practice in monitoring electrical machinery shaft misalignment generally utilises two accelerometer sensors, acting at 90° degree spatial displacement [38]. This reflects the fact that angular misalignment causes axial vibration at fundamental rotational frequency (f_r), while parallel misalignment produces radial vibration at twice the fundamental rotational speed frequency ($2f_r$): employing two accelerometers, one axially and the other radially mounted on the machine frame, to separately monitor axial and radial vibration signals allows for identification of effects caused by both types of misalignment and therefore its diagnosis.

The commercial misalignment detection systems undertake analysis of the captured vibration spectra to extract distinct identifiers of misalignment: it is widely acknowledged that most misalignment is a combination of offset and angular, hence both the f_r and $2f_r$ frequency components in both radial and axial vibration signals are observed for diagnosis purposes [37]. A common approach used in practice is to observe the ratio between the $2f_r$and f_r components' magnitudes, denoted in further text as $\mathrm{M}_2 f_r$ and $\mathrm{M}f_r$ respectively, in the frame acceleration signals, and observe its amplitude change. If misalignment is present in the system, a higher than normal (e.g. at healthy system conditions) value of the misalignment diagnostic index, where $m = |\mathrm{M}_2 f_r/\mathrm{M}f_r|$, is expected [39].

III. FBG Strain Sensing Principles and Sensor Design

An FBG sensor is small structure imprinted in a single mode optical fiber core. It is fabricated by creating a permanent periodic change (gratings) in the fiber core's refractive index by exposure the fiber core to an interference pattern of UV light [19]. The FBG sensor size is typically very small (i.e standard optical fiber size is ≈125 μm in diameter, while FBG head length typically range from 2 to 20 mm). In principle, a FBG sensor operates as a light filter that reflects a narrowband light wavelength when a fiber contains a FBG head is illuminated by broad band light source [40], [41].

The FBG head reflected wavelength is known as Bragg wavelength, λ_B, and can be defined as [21]:

$$\lambda_B = 2\Lambda n_{eff} \tag{6}$$

where Λ is the grating period and n_{eff} is the FBG's effective refractive index. These parameters alter with the variation in the temperature and strain exposed to FBG structure, thus altering the reflected narrowband wavelength. Assuming constant temperature, the variation in λ_B due to strain variation $\Delta\varepsilon$ can be expressed as [21]:

$$\Delta\lambda_B = 2\left(\Lambda\frac{dn_{eff}}{d\varepsilon} + n_{eff}\frac{d\Lambda}{d\varepsilon}\right)\Delta\varepsilon \tag{7}$$

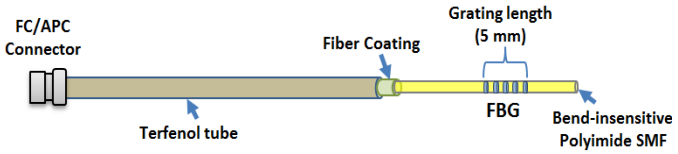

Fig. 3. FBG sensor schematic diagram.

The response of the FBG sensor to strain arises due to the change in the grating period (the physical elongation of the sensor), and the change in the reflective index due to photo-elastic effects. A typical theoretical value of strain sensitivity of a standard FBG imprinted with λ_B at 1500 nm is $\approx$1.2 pm/μ strain [19]. This value, however, can vary depending on the FBG sensor installation and packaging methods. The performance of surface strain sensing using FBG technology can be affected by the utilized bonding material and mounting procedure [41]. Different bonding methods have been explored in literature, ranging from application of cyanoacrylate adhesive and epoxy-resin glue [42], [43] to use of polyamide tape [19], [43]. While the former methods can provide increased rigidity and thus load to sensor transfer, they also impose a generally more complicated installation procedure and are fixed with no flexibility in terms of sensor repositioning and re-application. Polyamide tape bonding application on the other hand has been reported to provide good levels of measured load transfer from the structure to the sensor with advantage of high application flexibility; this method is used in the feasibility study reported in this work, as detailed further in section IV.B.

A schematic diagram of the FBG sensor design employed in this study is shown in Fig. 3. Each used sensor contains a 5 mm FBG head imprinted in a bend-insensitive fiber polyimide single mode optical fiber. The FBGs respective central Bragg wavelengths are at 1548 nm with average reflectivity of 80 % and a bandwidth of 0.3 nm. The sensor is applied for strain measurement in this work but is also inherently sensitive to thermal excitation. However, the thermal conditions rate of change in this application is much lower than that observed in frame strain, and should therefore allow clear differentiation of thermal and mechanical effects in the measurements: this will be further studied in experimental work in section V.

IV. Experimental System Setup

A. Test-Rig Facility

The experimental test rig comprises a purpose built DFIG system containing a three-phase, 415 V, four-pole 30kW wound rotor induction machine (WRIM) whose rotor windings are interfaced to the grid via a back-to-back voltage source converter formed by two CT UNIDRIVE SP-4401 units [45]. The DFIG is directly coupled to a 40kW DC load motor, which is controlled by a DC drive (CT MENTOR II) to enable establishment of a desired test load profile. A real-time stator flux oriented control (SFOC) routine is implemented on the rig using commercial converters by through a dSPACE 1103 real-time platform and the procedure reported in [43]. The DFIG is equipped with a suite of LEM LA 55P/SP1 current and LV 25-600 voltage Hall sensors to enable monitoring of

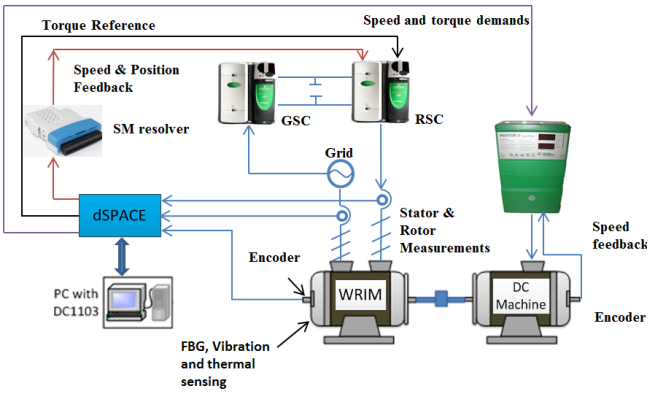

Fig. 4. Simplified schematic diagram of the laboratory test rig.

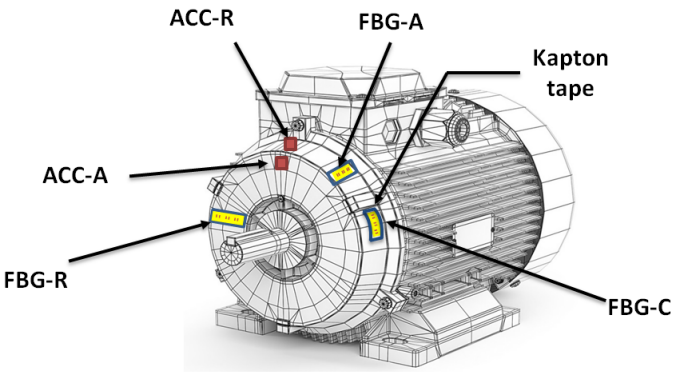

Fig. 5. Positions of FBG sensors and accelerometers.

relevant electrical signals, and a 1024 ppr incremental encoder for observing the rotor angular speed. A simplified schematic diagram of the test system is presented in Figure 4.

To enable vibration sensing according to accepted practice for misalignment [39] and its correlation to explored frame strain analysis, two Bruel &Kjaer (B&K) DT4394 piezoelectric accelerometers were installed on the generator's drive end plate|: one in the axial (ACC-A) and the other in the radial (ACC-R) orientation, as illustrated in Fig. 5. The accelerometer outputs were conditioned and analyzed using the B&K Pulse vibration monitoring platform. For the purpose of investigating the thermal effects on the proposed FBG strain measurements due to inherent FBG thermo-mechanical cross sensitivity the frame temperature was measured by installing a thermo-couple type K on the drive end-cap side of the test machine. The thermocouple is connected to Fluke T3000 digital thermometer type K.

B. Description of FBG Placement

Three different orientations of the frame FBG strain sensing were examined to enable understanding of optimal sensor positioning for misalignment recognition, as illustrated in Fig 5. FBG strain gauges were installed on the test machine frame in axial, radial and circumferential orientation, denoted in further text as FBG-A, FBG-R and FBG-C, respectively. All the used FBG sensors were non-invasively installed on the frame by bonding the respective sensing head to the surface of

the frame drive-end cap: FBG-A is placed on the top of end cap oriented parallel to the motor shaft, FBG-R is mounted on the end cap side in orientation perpendicular to the motor shaft, and FBG-C is fitted along the end cap round external surface. To ensure optimum strain gauge bonding the frame surface in target sensing areas was first stripped of paint, then smoothed by fine sand paper and finally cleaned with Isopropyl alcohol before attaching the FBG sensors, following the procedure applied in [19], [43]. The FBG sensing heads were bonded to the treated frame surface by means of Kapton tape [19].

C. Examined Angular Misalignment Conditions

For the purpose of this study two different severities of angular shaft misalignment were practically emulated on the experimental test rig: this included operation in aligned conditions, and with one degree and three degree shaft misalignment. The desired misalignment levels were achieved by introducing appropriately dimensioned shims under the feet of the test motor. A commercial TKSA 51 laser alignment tool was then used to verify the correct amount of misalignment has been achieved on the experimental system. The alignment tool was also used to ascertain there is no offset alignment present in the system during tests.

V. Experimental Results and Discussion

A range of experiments were undertaken to evaluate the proposed FBG frame strain sensing network efficacy in enabling recognition of angular misalignment. To this end the findings obtained from FBG sensor measurements are cross compared with those from a commercial vibration monitoring platform.

The laboratory DFIG was tested at the following four operating speeds covering both its sub- and super-synchronous operating ranges: 1340 rpm, 1440 rpm 1550 rpm and 1590 rpm. For each considered speed point, three different load levels were examined by performing tests at 25%, 50% and 100% nominal load (current). For each examined speed and load condition three separate test were undertaken, with the DFIG operating with an aligned shaft and 1 and 3 degrees of angular misalignment. A set of thermal tests were also carried out to investigate the FBG thermo-mechanical cross sensitivity effects and ascertain sensors capability for long term online application and how their measurements are affected by the inherent machine surface temperature change.

The findings are presented in the following subsections. Sections A and B focus on exploring the nature of fault related content manifestation in the observed signals spectra for a single operating point, to illustrate the frequency domain content recorded by the strain sensors. Section C then undertakes a consistency study of the identified behavior on a wider range of operating points. Finally, section D presents the results of the thermos-mechanical cross sensitivity study.

A. Strain and Vibration Signals Spectral Content Analysis

The typical spectral content observed in the evaluated frame strain and acceleration measurements is shown in detail for an illustrative DFIG operating point (1340 rpm, 25% load) and the examined misalignment conditions in this section to enable understanding of FBG strain monitoring potential.

The measured strain and vibration time domain signals were processed in 2^{17} FFT routines to extract the corresponding spectral content. The resulting data are shown in Fig. 6 for the *0* to *110* Hz bandwidth to enable a relatively wide band comparison of the spectral content observed by strain and acceleration sensors. While, generally, the fundamental and second order harmonics are typically monitored for misalignment analysis purposes [39], rotational speed harmonics of up to 4th order are examined in this section for the sake of validating the FBG strain sensor capability of registering misalignment induced frame strain components corresponding to those seen in vibration measurements.

The numeric values of the first four f_r harmonic frequencies at the examined speed (given by: $f_{rk} = kxn_r/60Hz$), where $k = 1, 2, 3\ldots$ and n_r is the rotor speed in (rpm) are: 22.33 Hz, 44.67 Hz, 66.99 Hz and 89.33 Hz. The measured strain and vibration data in Fig. 6 clearly report the presence of these components, with similar general spectral contents trends observed in healthy and fault conditions. The comparison of the three different orientation frame strain FBG measurements reveals that strong f_{rk} peaks are present in both axial and circumferential strain signals, while the radial strain measurements are considerably less significant in comparison; this suggests lower sensitivity of strain measurements in radial orientation. Compared to the vibration measurements, the strain signals are seen to report more clearly pronounced f_{rk} components in spectra containg a generally lower noise level.

B. Fault Related Component Analysis

This section undertakes a detailed cross correlation study of the strain and vibration signals fault related components, i.e. the fundamental and the second order rotational speed harmonics. To this end, the magnitudes of the strain and vibration signals' f_r and $2f_r$ frequency components measured in Fig. 6 are summarised in Appendix Table I.

The measurements in Table I demonstrate that no consistent magnitude change with fault level increase can be observed in the FBG measured f_r and $2f_r$ components. As a result, observing the individual magnitude only of these components is not suitable for provision of diagnostic knowledge on angular shaft misalignment. Similarly, the vibration signals exhibit a general inconsistency in the behaviour of the observed f_r and $2f_r$ components magnitude at different fault levels making it challenging to utilise these for deriving reliable diagnostic information: while some consistence with fault level propagation can be observed in isolated cases (e.g $2f_r$ component in the radial vibration spectrum) this does not hold for other load and speed conditions.

Therefore, the commonly used misalignment diagnostic index, based on the magnitude ratio of the 2nd and 1st harmonic (m, as defined in section II.B) has been applied on the measured data and the obtained index values summarised in Appendix Table II. The introduction of the ratio index m significantly alters the diagnostic potential of the analysed frame strain and vibration measurements. Regarding the FBG strain signals, it can be observed that the index m continuosly increases with fault level increase in both the axial and

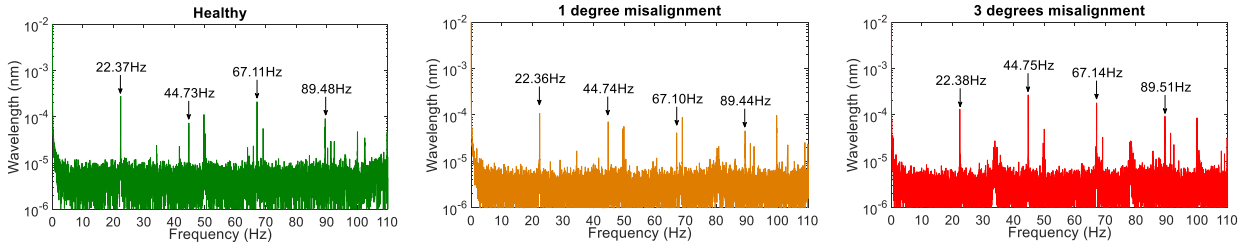

A. FBG axial strain measurement FFT spectrum for different conditions

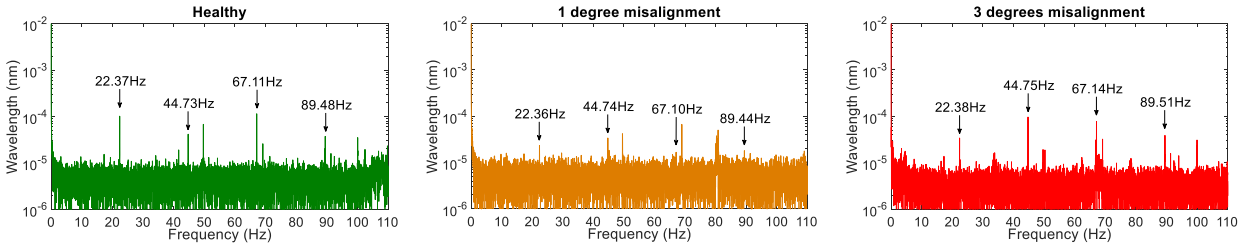

B. FBG circumferential strain measurement FFT spectrum for different conditions

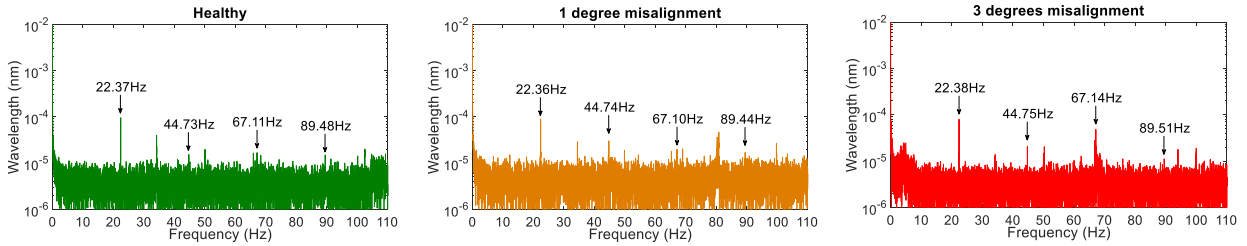

C. FBG radial strain measurement FFT spectrum for different conditions

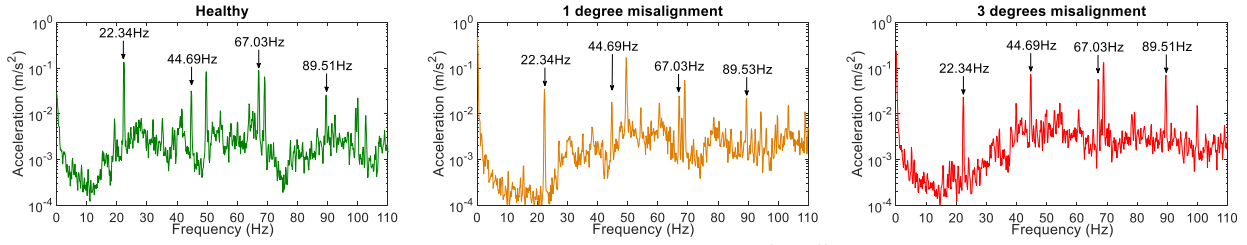

D. Accelerometer axial measurement FFT spectrum for different conditions

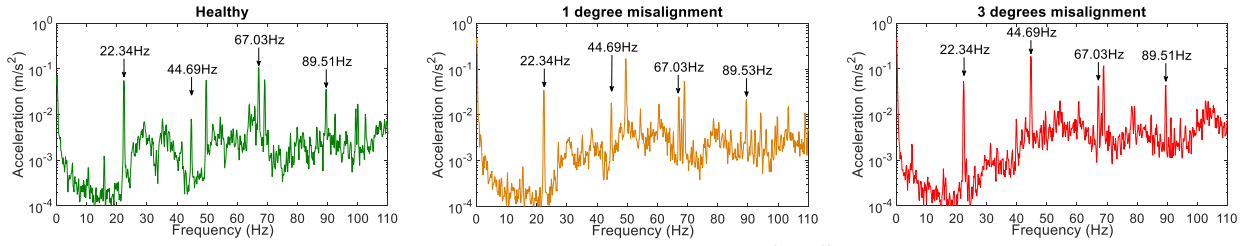

E. Accelerometer radial measurement FFT spectrum for different conditions

Fig. 6. FBG strain and vibration signals spectrum in different severities of shaft misalignment at DFIG 1340 rpm 25% load condition.

circumferential direction measurements (FBG-A and FBG-C); nevertheless, this trend could not be monitored in the FBG-R signal, reflecting the observations on the lower sensitivity of measurement taken in this orientation to fault, reported in section V.A. Similarly, a continuous growth in the index m value is seen in both axial and radial vibration signal measurement, as is generally expected [39]. The reported measurements indicate that in-situ frame strain sensing has comparable diagnostic potential to conventional frame vibration monitoring, depending on the sensing orientation: both FBG-A and FBG-C are demonstrated to enable clear recognition of the presence and magnitude of angular shaft misalignment.

C. Diagnostic Consistency Study in the Wider Operating Range

This section examines the consistency of the diagnostic index manifestation in the frame strain measurements observed in section V.B over a wider range of generator operating points

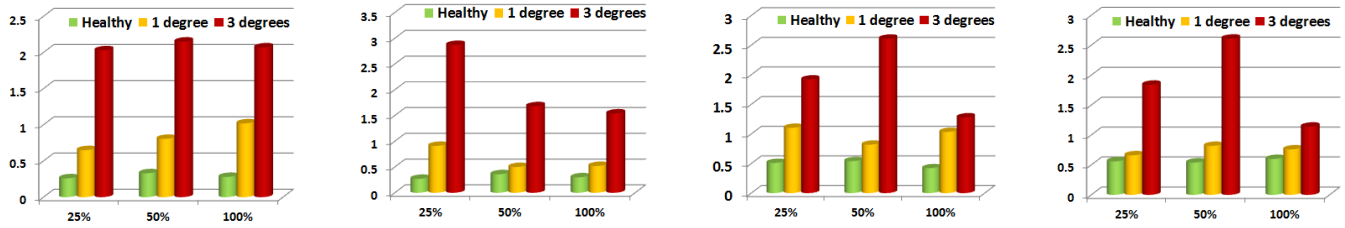

(a) 1340 rpm (b) 1440 rpm (c) 1550 rpm (d) 1590 rpm

Fig. 7. Measured value of diagnostic index *m* in axial strain.

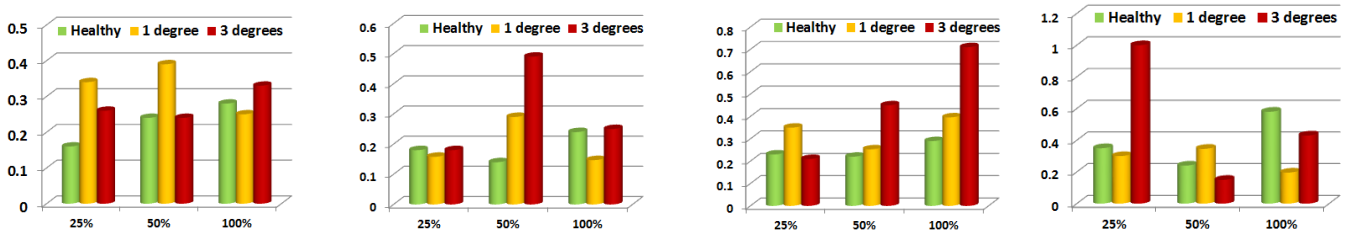

(a) 1340 rpm (b) 1440 rpm (c) 1550 rpm (d) 1590 rpm

Fig. 8. Measured value of diagnostic index *m* in radial strain.

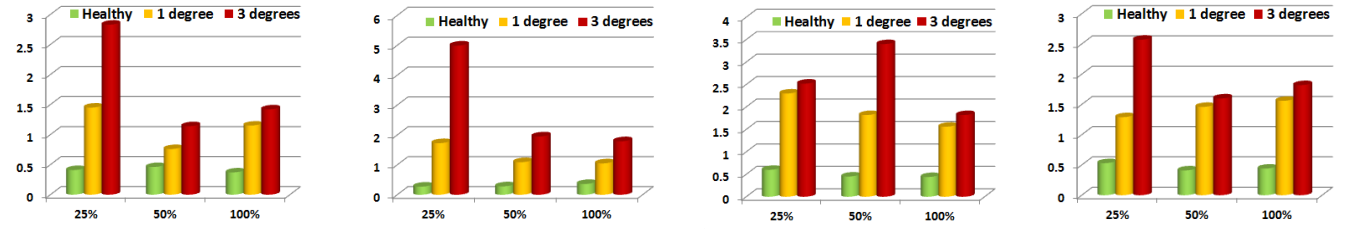

(a) 1340 rpm (b) 1440 rpm (c) 1550 rpm (d) 1590 rpm

Fig. 9. Measured value of diagnostic index *m* in circumferential strain.

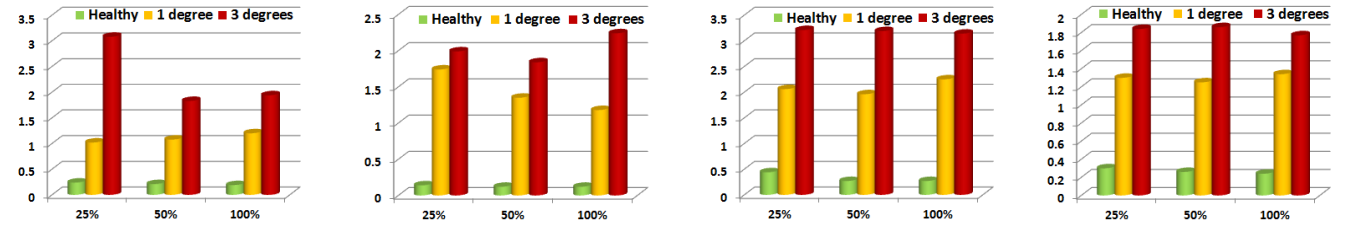

(a) 1340 rpm (b) 1440 rpm (c) 1550 rpm (d) 1590 rpm

Fig. 10. Measured value of diagnostic index *m* in axial vibration.

and loads, representative of its field application conditions. The misalignment diagnostic index values obtained from the axial, radial and circumferential direction frame strain measurements for the four examined speeds at loads and fault levels detailed in section V introduction are shown in Figs. 7-9. The corresponding axial and radial vibration measurements are presented in Figs. 10 and 11.

The index measurements in Figs. 7-9 show that, as observed in sections V.A and V.B, the radial direction strain (Fig. 8) exhibits an incosistent *m* behaviour with fault level variation; radial strain would generally be expected to be more sensitive to offset misalignment, and while, as such, this signal is not of direct use for diagnosis of angular misalignment severity, it could potentially be used to differentiate the type of misalignment observed in the system using frame strain measurements. The axial and circumferential strain measurements on the other hand are seen to report clear increase trends in *m* value for all examined conditions: both these signals could enable unambiguous detection of angular misalignment presence and monitoring its level propagation. While both signals exibit strong sensitivity to fault presence and level, it can be observed that circumferential strain provides increased sensitivity to lower fault levels, while axial strain is more responsive to high level fault. The misalignment diagnosis performance

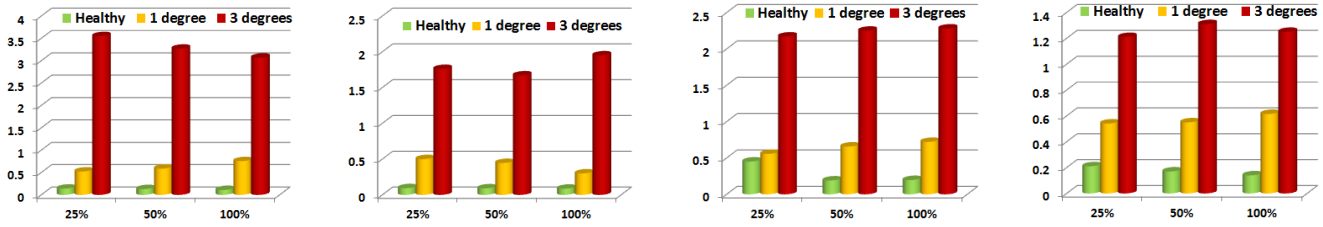

(a) 1340 rpm (b) 1440 rpm (c) 1550 rpm (d) 1590 rpm

Fig. 11. Measured value of diagnostic index m in radial vibration.

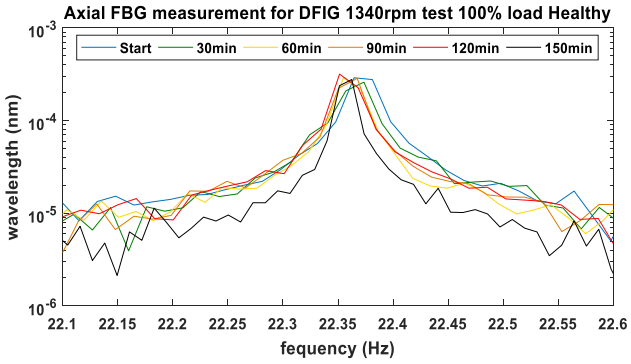

Fig. 12. Measured thermal variation caused change in f_r component of FBG-A spectrum.

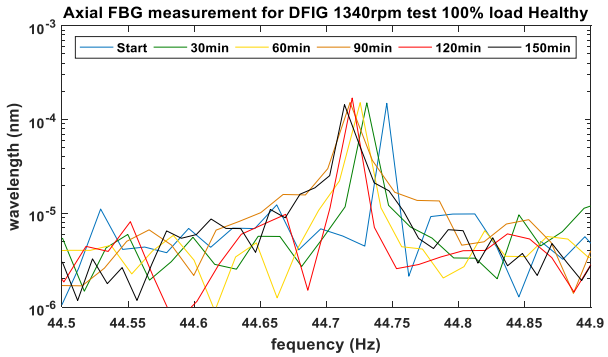

Fig. 13. Measured thermal variation caused change in $2f_r$ component of FBG-A spectrum.

could therefore be strenghtened by the joint use of these two, allowing for an increased sensitivity across the fault level spectrum. Finally, comparison with the corresponding vibration measurements in Figs. 10 and 11 demonstrates that the diagnostic performance provided by FBG frame strain sensing is comparable to that attainable using conventional frame vibration monitoring.

D. Thermal Cross-Sensitivity Effects Evaluation

The FBG sensors are intrinsically sensitive to both strain and thermal excitation variation. It is thus necessary to investigate how the proposed frame FBG strain sensing is affected by machine surface temperature change in long terms tests emulating thermal conditions encountered in practial use. To this end, the test DFIG was operated at 100% nominal current at 1340 rpm in healthy conditions for an extended time period to allow for the machine frame temperature to attain its steady-state nominal load level. The test was run for approximately 150 min to ensure the steady-state thermal equilibrium is reached. The frame surface temperature in the vicinity of FBG sensors and the axial and circumferential direction strain, demonstrated to enable recognition for angular misalignment in previous sections, were measured at every 30 minutes during the test.

To illustrate the observed strain changes due to frame temperature change the measured f_r and $2f_r$ components magnitudes in the axial strain signal spectrum are shown in Fig. 12 and Fig. 13, respectively. The corresponding frame temperature measurements are shown in Fig. 14: at test start the frame was at ambient temperature (≈26.3°C), reaching

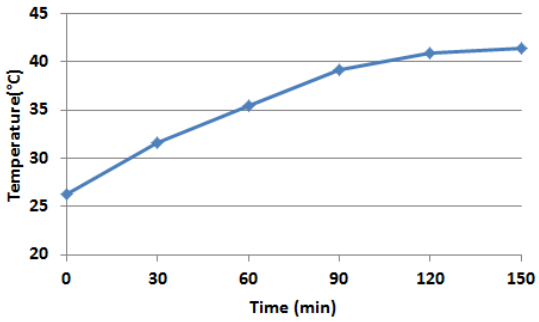

Fig. 14. Measured generator frame temperature rise from thermal ambient to thermal steady-state value at 1340rpm, 100% load.

a steady-state temperature of ≈41.4°C at test end. The presented experimental data in Fig. 12 and 13 demonstrate that the f_r and $2f_r$ components exhibit a relatively minor change in magnitude (measured at a maximum of 0.0000573nm for f_r magnitude variation and 0.0000573nm for $2f_r$ variation).

The measured maximum variation in the axial and circumferential strain measurements caused by the frame temperature change was used to map the deviation of the corresponding values of diagnostic index m, and the results shown in Fig. 15. The blue and red bars in Fig. 15 represent the minimum and maximum observed m values during the 150 min test duration. To enable evaluation of the significance of the thermal induced change in the diagnostic index, the value of m measured for 1 degree fault condition in Fig. 7 is also shown in the figures, and is represented by a black line. The measured data report the m variation range for FBG-A of 0.29 to 0.52,

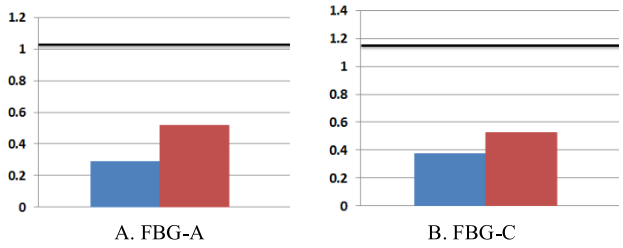

Fig. 15. Frame temperature variation induced change in *m* index value - measured in ambient to thermal steady-state rise tests at 1340rpm, 100% load.

which is much lower than the index value for 1 degree fault condition. Similarly, the range of FBG-C variation in *m* is from 0.38 to 0.5, while the 1 degree fault condition index value is 1.15. In summary, the thermo-mechanical cross-sensitivity test results indicate that no observable detrimental effect can be identified on the diagnostic performance of FBG frame strain measurements for recognition of angular misalignment; while thermal induced changes in the relevant diagnostic index values are present with change in thermal conditions on the frame, these are seen to be of relatively insignficant magnitude and do not compromise the ability of strain measurement to enable recognition of misalignment conditions.

VI. Conclusions

This paper presents an FBG strain sensor application study for monitoring and diagnosis of misalignment conditions in electric machine drivetrains, based on observation of machine frame relative strain. The proposed method enables straightforward retrofit to existing machinery, and is shown to have the capability to provide an effective means of distributed measurement and monitoring of misalignment induced effects.

The reported technique's performance was evaluated in laboratory tests on a purpose built doubly-fed induction generator test facility, allowing controlled introduction of desired level of angular misalignment. The findings demonstrate that the proposed FBG strain measurements on the generator frame surface can enable recognition and trending of misalignment fault presence and level, and provide diagnostic capability that is commonly obtained through application of more complicated conventional acceleration monitoring systems. It was also found that the FBG sensor innate thermo-mechanical cross sensitivity combined with frame surface temperature variation that is inherent to electric machine operation, has no detrimental effect on the observation of frame signal embedded misalignment signature. The diagnostic potential of differing in-situ FBG strain observation for diagnosis of angular misalignment was assessed, showing that both angular and circumferential direction measurements are strongly responsive to fault presence. Further investigation of optimizing the sensor surface bonding to yield enhanced load to sensor transfer could provide improvements on the reported findings.

Compared to application of accelerometer sensors that exclusively monitor mechanical effects the reported scheme can provide additional thermal monitoring capability utilizing

TABLE I
Measured f_r and $2f_r$ Frequency Components' Magnitudes in Frame Strain and Acceleration Spectra at 1340 rpm and 25% Load

Signal source	f_r magnitude			$2f_r$ magnitude		
	H	1°	3°	H	1°	3°
FBG-A (nm)	$28\text{x}10^{-5}$	$11\text{x}10^{-5}$	$13\text{x}10^{-5}$	$7.3\text{x}10^{-5}$	$7.1\text{x}10^{-5}$	$27\text{x}10^{-5}$
FBG-C (nm)	$10\text{ x}10^{-5}$	$2.3\text{x}10^{-5}$	$3.4\text{x}10^{-5}$	$4.2\text{x}10^{-5}$	$3.4\text{x}10^{-5}$	$9.7\text{x}10^{-5}$
FBG-R (nm)	$9.6\text{x}10^{-5}$	$8.9\text{x}10^{-5}$	$8.0\text{x}10^{-5}$	$1.5\text{x}10^{-5}$	$3.0\text{x}10^{-5}$	$2.1\text{x}10^{-5}$
Axial vibration (m/s^2)	0.13	0.021	0.023	0.031	0.021	0.073
Radial vibration (m/s^2)	0.055	0.034	0.053	0.0079	0.018	0.19

TABLE II
Measured Value of Diagnostic Index *m* at 1340 rpm and 25% Load

Signal source	m		
	H	1°	3°
FBG-A	0.26	0.65	2.03
FBG-C	0.41	1.45	2.83
FBG-R	0.16	0.34	0.26
Axial vibration	0.24	1.02	3.18
Radial vibration	0.14	0.52	3.55

the same hardware platform due to FBG inherent multi-physical sensing capability. Further advantages can also be derived from its ease of installation and positioning, the fact it is power passive, as well as its capability to be integrated into wider FBG multi-sensor systems allowing all-inclusive electrical machine condition monitoring and replacing the current practice where a suite of disparate single-physics sensors is applied for this purpose (e.g., current, temperature, vibration etc.). Finally, the scheme offers full EMI immunity as is inherent to FBG sensing which is important in EMI rich electric machine applications and requires additional measures to achieve in conventional sensor alternatives. While further exploration is needed, the presented principles could enable the development of electric machinery misalignment detection schemes based on distributed in-situ FBG strain sensing of machine frame, as standalone systems or as part of wider drivetrain FBG monitoring schemes.

Finally, the FBG sensor cost is currently comparable to cost of conventional lower grade piezoelectric accelerometers, and considerably lower than the cost of high end commercial vibration sensors. The required FBG interrogator systems however remain costly, and although more expensive compared to low end charge amplifier/signal conditioning systems for accelerometer platforms they compare favorably in cost to high end accelerometer conditioning systems. The interrogator cost in practical applications could nevertheless potentially be offset by intelligent exploitation of the FBG multi-physical

sensing capability and multiplexing to yield an integrated monitoring system with much greater CM functionality compared to vibration only monitoring platforms.

APPENDIX

See Tables I and II.

REFERENCES

[1] *Offshore Wind Outlook 2019*. Int. Energy Agency, Paris, France, Nov. 2019.

[2] *UpWind-Design Limits and Solutions for Very Large Turbines*, Eur. Wind Energy Assoc., EWEA, Brussels, Belgium, 2011.

[3] *Installation, Operation & Maintenance Strategies to Reduce the Cost of Offshore Wind Energy*, NREL, Golden, CA, USA, 2013.

[4] G. Hassan, *Guide to UK Offshore Wind Operations and Maintenance*, Crown Estate, London, U.K., 2013.

[5] *Certification of Condition Monitoring, Service Specification*, document DNVGL-SE-0439-Edition, Jun. 2016.

[6] Yang, Wenxian, Peter J. Tavner, Christopher J. Crabtree, Y. Feng, and Y. Qiu, "Wind turbine condition monitoring: Technical and commercial challenges," *Wind Energy*, vol. 17, no. 5, pp. 673–693, 2014.

[7] *Certification of Condition Monitoring, Service Specification*, document DNVGL-SE-0439, Jun. 2016.

[8] *Vibration Diagnostic Guide. SKF Reliability Systems*, document CM5003, 2000.

[9] G. Knitz, "A guide to wind turbine alignment," Wind Systems Magazine, Mar. 2012, pp. 22–25.

[10] O. Tonks and Q. Wang, "The detection of wind turbine shaft misalignment using temperature monitoring," *CIRP J. Manuf. Sci. Technol.*, vol. 17, pp. 71–79, May 2017.

[11] *Guideline for the Certification of Condition Monitoring Systems for Wind Turbines*, Germanischer Lloyd Renewables Certification, Hamburg, Germany, 2013.

[12] S. Sheng *et al.*, "Wind turbine drivetrain condition monitoring during GRC phase 1 and phase 2 testing," Nat. Renew. Energy Lab., Golden, CO, USA, 2011.

[13] *Maintenance*, Skill Wind, Eur. Comission Erasmus+Programme, Brussels, Belgium, 2015.

[14] R. R. Obaid, T. G. Habetler, and R. M. Tallam, "Detecting load unbalance and shaft misalignment using stator current in inverter-driven induction motors," in *Proc. IEEE Int. Electr. Mach. Drives Conf. (IEMDC)*, Madison, WI, USA, vol. 3, 2003, pp. 1454–1458.

[15] W. Zhang, J. Yang, C. Li, R. Dai, and A. Yang, "Theoretical and experimental research on turbo-generator shaft alignment using strain gauge method," *J. Vib. Control*, vol. 23, no. 7, pp. 1183–1192, Apr. 2017.

[16] A. Simm, Q. Wang, S. Huang, and W. Zhao, "Laser based measurement for the monitoring of shaft misalignment," *Elsevier Meas.*, vol. 87, pp. 104–116, Jun. 2016.

[17] K. M. Sousa, U. J. Dreyer, C. Martelli, and J. C. Cardozo da Silva, "Dynamic eccentricity induced in induction motor detected by optical fiber Bragg grating strain sensors," *IEEE Sensors J.*, vol. 16, no. 12, pp. 4786–4792, Jun. 2016.

[18] K. M. Sousa, I. Brutkowski Vieira da Costa, E. S. Maciel, J. E. Rocha, C. Martelli, and J. C. Cardozo da Silva, "Broken bar fault detection in induction motor by using optical fiber strain sensors," *IEEE Sensors J.*, vol. 17, no. 12, pp. 3669–3676, Jun. 2017.

[19] A. Mohammed, N. Sarma, and S. Djurovic, "Fibre optic monitoring of induction machine frame strain as a diagnostic tool," in *Proc. IEEE Int. Electric Mach. Drives Conf. (IEMDC)*, Miami, FL, USA, May 2017, pp. 1–7.

[20] A. Mohammed and S. Djurovic, "Stator winding internal thermal monitoring and analysis using *in situ* FBG sensing technology," *IEEE Trans. Energy Convers.*, vol. 33, no. 3, pp. 1508–1518, Sep. 2018.

[21] A. Mohammed, J. I. Melecio, and S. Djurovic, "Stator winding fault thermal signature monitoring and analysis by *in situ* FBG sensors," *IEEE Trans. Ind. Electron.*, vol. 66, no. 10, pp. 8082–8092, Oct. 2019.

[22] A. Mohammed, J. I. Melecio, and S. Djurovic, "Open-circuit fault detection in stranded PMSM windings using embedded FBG thermal sensors," *IEEE Sensors J.*, vol. 19, no. 9, pp. 3358–3367, May 2019.

[23] J. P. V. Fracarolli *et al.*, "Development and field trial of a FBG-based magnetic sensor for large hydrogenerators," *Proc. SPIE*, vol. 9852, May 2016, Art. no. 98520L.

[24] G. Bieler and M. M. Werneck, "A magnetostrictive-fiber Bragg grating sensor for induction motor health monitoring," *Measurement*, vol. 122, pp. 117–127, Jul. 2018.

[25] A. Mohammed, J. I. Melecio, and S. Djurović, "Electrical machine permanent magnets health monitoring and diagnosis using an air-gap magnetic sensor," *IEEE Sensors J.*, to be published.

[26] A. Mohammed and S. Djurovic, "*In-situ* thermal and mechanical fibre optic sensing for in-service electric machinery bearing condition monitoring," in *Proc. IEEE Int. Electr. Mach. Drives Conf. (IEMDC)*, San Diego, CA, USA, May 2019, pp. 37–43.

[27] M. Fabian, D. M. Hind, C. Gerada, T. Sun, and K. T. V. Grattan, "Comprehensive monitoring of electrical machine parameters using an integrated fiber Bragg grating-based sensor system," *J. Lightw. Technol.*, vol. 36, no. 4, pp. 1046–1051, Feb. 15, 2018.

[28] T. Erdogan, "Fiber grating spectra," *J. Lightw. Technol.*, vol. 15, no. 8, pp. 1277–1294, 1997.

[29] K. O. Hill and G. Meltz, "Fiber Bragg grating technology fundamentals and overview," *J. Lightw. Technol.*, vol. 15, no. 8, pp. 1263–1276, 1997.

[30] M. Xu and R. D. Marangoni, "Vibration analysis of a motor-flexible coupling-rotor system subject to misalignment and unbalance, part I: Theoretical model and analysis," *J. Sound Vib.*, vol. 176, no. 5, pp. 663–679, Oct. 1994.

[31] J. M. Bossio, G. R. Bossio, and C. H. De Angelo, "Angular misalignment in induction motors with flexible coupling," in *Proc. 35th Annu. Conf. IEEE Ind. Electron.*, Porto, Portugal, Nov. 2009, pp. 1033–1038.

[32] P. F. S. E. A. B. Ursula Ferraz, "A simplified model for mechanical loads under angular misalignment and unbalance," *Int. J. Mech., Aerosp., Ind., Mech. Manuf. Eng.*, vol. 7, no. 7, pp. 1611–1617, 2013.

[33] I. Porat, "Moment transmission by a universal joint," *Mechanism Mach. Theory*, vol. 15, no. 4, pp. 245–254, Jan. 1980.

[34] S. Djurović, D. S. Vilchis-Rodriguez, and A. C. Smith, "Investigation of wound rotor induction machine vibration signal under stator electrical fault conditions," *J. Eng.*, vol. 2014, no. 5, pp. 248–258, May 2014.

[35] P. Rodriguez, A. Belahcen, and A. Arkkio, "Signatures of electrical faults in the force distribution and vibration pattern of induction motors," *IEE Proc.-Electr. Power Appl.*, vol. 153, no. 4, pp. 523–529, 2006.

[36] S. K. F. R. Systems. (SKF). *SKF Reliability Systems Vibration Diagnostic Guide CM5003*. Accessed: Sep. 1, 2019. [Online]. Available: http://edge.rit.edu/edge/P14453/public/Research/SKF VibrationGuide.pdf

[37] J. B. A. Bilosova, "Vibration diagnostics," in *Investments in Education Development Book*. Ostrava, Czech Republic, 2012.

[38] J. S. U. I. Mais. (2012). *Spectrum Analysis, The Key Features of Analysing Spectra*. Accessed: Aug. 22, 2019. [Online]. Available: https://www.skf.com/binary/tcm:12-113997/CM5118%20EN%20Spectrum%20Analysis.pdf

[39] A. Othonos, "Fiber Bragg gratings," *Rev. Sci. Instrum.*, vol. 68, no. 12, pp. 4309–4341, 1997.

[40] R. Kashyap, *Fiber Bragg Gratings*. New York, NY, USA: Academic, 2009.

[41] P. Motwani, N. Perogamvros, S. Taylor, M. Sonebi, A. Laskar, and A. Murphy, "Experimental investigation of strain sensitivity for surface bonded fibre optic sensors," *Sens. Actuators A, Phys.*, vol. 303, Mar. 2020, Art. no. 111833.

[42] B. P. Alalibo, W. P. Cao, A. Gbadebo, L. Aarniovuori, and K. Cai, "Investigation of the effect of bonding points on metal surface-mounted FBG sensors for electric machines," *Prog. Electromagn. Res.*, vol. 97, pp. 255–265, Aug. 2019.

[43] I. Grabovac, T. Nuyens, and C. Davis, "Packaging and mounting of in-fibre Bragg grating arrays for structural health monitoring of large structures," Defence Sci. Technol. Org., Melbourne, SA, Australia, Tech. Rep. DSTO-TR-2490, 2010.

[44] S. Djurovic, D. S. Vilchis-Rodriguez, and A. C. Smith, "Supply induced interharmonic effects in wound rotor and doubly-fed induction generators," *IEEE Trans. Energy Convers.*, vol. 30, no. 4, pp. 1397–1408, Dec. 2015.

[45] N. Sarma, P. M. Tuohy, J. M. Apsley, Y. Wang, and S. Djurović, "DFIG stator flux-oriented control scheme execution for test facilities utilising commercial converters," *IET Renew. Power Gener.*, vol. 12, no. 12, pp. 1366–1374, Sep. 2018.

Yingzhao Wang received the B.Eng. degree in electrical engineering from the University of Liverpool, U.K. He is currently pursuing the Ph.D. degree in electrical engineering with the University of Manchester. His research interests are in electric machines condition monitoring, control, and real-time estimation techniques.

Anees Mohammed received the M.Sc. degree in electrical power engineering from the University of Newcastle, U.K., in 2010, and the Ph.D. degree in electrical and electronic engineering from the University of Manchester, U.K., in 2019.

He is currently a Research Associate with the Power Conversion Group, University of Manchester. He spent four years working as an Assistant Lecturer at Benghazi University, Libya. His research interests are in electric machines, drives, and condition monitoring.

Nur Sarma received the Ph.D. degree in electrical engineering from the University of Manchester in 2017. She is currently an Associate Professor with Düzce University, Turkey. Her research interests are in electric machines, drives, and condition monitoring.

Siniša Djurović (Member, IEEE) received the Dipl.-Ing. degree in electrical engineering from the University of Montenegro in 2002 and the Ph.D. degree in electrical and electronic engineering from the University of Manchester in 2007.

He is currently a Senior Lecturer with the Power Conversion Group, University of Manchester. His research interests are in the area of operation, design, monitoring, and diagnostics of electric machines and drives.